TURBULENT BOUNDARY LAYER FLOW OVER CIRCULAR CAVITIES

J. Dybenko, T. Hering, E. Savory
Department of Mechanical and Materials Engineering, The University of Western Ontario

Keywords: *Cavity, Circular, Wake Flow, Feedback Resonance, Asymmetry*

Abstract

Increasingly stringent emission standards for commercial aircraft engines will require a greater focus on airframe drag and noise reduction techniques. One source of drag that may be reduced is that due to the presence of cavities on aircraft surfaces such as rivet depressions and landing gear wheel wells. In order to gain a greater understanding of the causes of the drag related to such cavities, turbulent flow over circular cavities has been experimentally investigated in a subsonic wind tunnel.

Velocity measurements acquired in the cavity wake, using hot-wire anemometry, together with pressure measurements on the cavity surfaces show a link between the flow in the cavity and that in its wake. Oscillations in the pressure and velocity time series for a cavity depth to diameter ratio (h/D) ≈ 0.5 demonstrated a consistent peak at a frequency expected for the cavity feedback resonance mechanism. Since this peak was not observed at other depth configurations, cavity feedback resonance may be a cause for the high level of flow asymmetry and cavity drag observed for h/D ≈ 0.5. Good agreement was noted between the present experimental results and those from previous investigations.

1 Introduction

Investigations of the flows over surface-mounted cavities have been quite common due to their fundamental nature. Most of our understanding of these cavity flows has arisen from studies of cavities with rectangular planforms. There have been far fewer investigations of other geometries, such as the circular cavities examined in the present paper.

Rossiter simplified the understanding of cavity-related flow oscillations by dividing them into three categories: fluid-elastic, fluid-resonant and fluid-dynamic oscillations [1]. Fluid-elastic oscillations occur when a cavity surface itself is forced into oscillation, fluid-resonant oscillations are caused when a self-sustaining oscillation in the flow has a wavelength of the same order as one of the cavity dimensions, and fluid-dynamic oscillations relate to the cavity feedback resonance mechanism defined below.

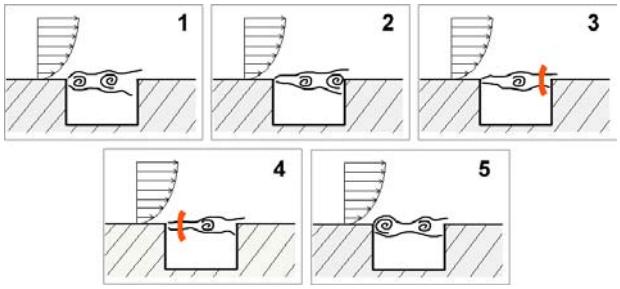

Fig. 1. Step-wise illustration of the cavity feedback resonance mechanism.

Rossiter also made another critical conceptual contribution to the study of oscillations resulting from cavity flows with his proposal of the fluid-dynamic mechanism for production of oscillations [1] which has since been confirmed by experiment [2, for example]. This phenomenon is often referred to as cavity feedback resonance and is illustrated in Figure 1. A vortex is shed from the upstream cavity lip (1) and is then convected downstream (2) towards the downstream lip where it impinges causing the generation of an acoustic pressure

pulse (3) that radiates upstream (4) and disturbs the shear layer at the upstream cavity lip causing another vortex to be shed (5).

Due to the self-sustaining nature of this feedback mechanism, acoustic pulses are generated periodically and a narrow-band acoustic tone results. Rossiter also developed an empirical formula to predict the frequency of this tone:

$$f = \frac{U_0(m-\gamma)}{l(M+1/\kappa)} \qquad (1)$$

Where f is the predicted frequency of oscillation.

It has been shown that this phenomenon also drastically increases the drag due to the cavity presence, by up to 250%, when compared to a cavity under similar conditions not undergoing this type of resonance [3].

Fluid-resonant oscillations are often observed in the flow over circular cavities, a phenomenon somewhat related to the Helmholtz resonance tone heard when blowing across the mouth of a bottle. Oscillations driven by this fluid-resonant mechanism can be predicted using the following equation for air column vibration in open cylinders [4]:

$$f = \frac{Nc}{4(h+0.3D)} \qquad (2)$$

which predicts a frequency that varies inversely with cavity depth.

A schematic diagram of circular cavity geometry is seen in Figure 2. Several differences have been noted between the flow over cavities of circular planform and those of rectangular and elliptical planform. For instance, when comparing their drag for various depth to streamwise length ratios (h/l) similar drag trends are observed at most depths, but for h/l equal to about 0.5 the circular case has a far greater drag than the rectangular or elliptical cases [5]. Along with the peak in drag noted at this configuration, a strong asymmetry about the stream-wise central axis of the cavity is also seen in the mean pressure distribution along the cavity surfaces [5]. This phenomenon marks a rare instance for which a highly asymmetric mean pressure distribution is found for a symmetric geometry. Gaudet and Winter [6] later discovered that the flow at most circular cavity depth configurations (usually stated in terms of the cavity depth to diameter ratio: h/D) consisted of a single large recirculation vortex with axis perpendicular to the stream-wise centreline of the cavity and rooted to opposite sides of the cavity inner sidewall. However, for the case of h/D ≈ 0.5 the axis of the recirculation vortex appeared at about 45° to the streamwise centreline and was only rooted to one point on the upstream cavity sidewall, such that the vortex axis angled upwards and exited the cavity at the downstream edge to form a trailing vortex downstream of the cavity [6]. The investigators reasoned that the peak in the drag noted at this depth was due to the exposed recirculation vortex sweeping more fluid into the cavity.

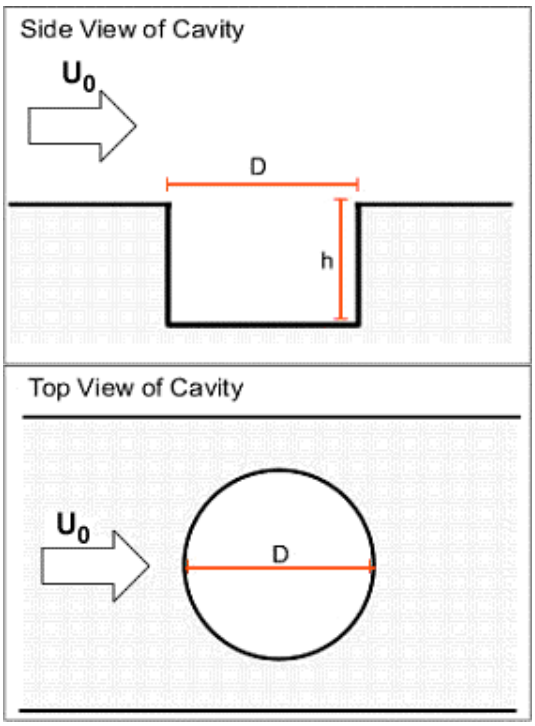

Fig. 2. Schematic diagram of circular cavity geometry.

Hiwada et. al. proposed a set of flow regimes based on the h/D ratio of the cavity by observing mean pressure patterns along the cavity surfaces, along with the shape of the pressure time series at points on the cavity surfaces at these various depth configurations

[7]. Pressures for these types of flows are often stated in terms of a pressure coefficient Cp, defined in equation (3) or for fluctuating pressures, Cp_{RMS}, defined in equation (4). This allows a presentation of the measured pressures in relation to the free stream dynamic pressure.

$$Cp = \frac{p - p_s}{\frac{1}{2}\rho U_0^{\,2}} \qquad (3)$$

$$Cp_{RMS} = \frac{\sqrt{(p - \overline{p})^2}}{\frac{1}{2}\rho U_0^{\,2}} \qquad (4)$$

Single spanwise lines of mean streamwise velocity [7,8] and turbulence [8] were also reported and these results served as further evidence for asymmetric mean flow for h/D 0.5 and symmetric mean flow for other depths.

The aims of the present study have been to find an explanation for the high drag and mean flow asymmetry noted for h/D ≈ 0.5 and to investigate the fluctuating nature of the flows at various depth configurations.

sample article is to show you how to prepare and submit papers in a standard style for electronic publishing in the ICAS 2006 CD ROM proceedings. It illustrates the paper layout, and describes points you should notice before you submit your papers.

2 Experimental Details

2.1 General Setup

Experiments were carried out in a closed-loop, subsonic wind tunnel in the Boundary Layer Wind Tunnel Laboratory (BLWTL) at the University of Western Ontario. The tunnel had working section dimensions of 6.50 m length 0.61 m width 0.21 m height. A free-stream velocity of 27.0 m/s was used for testing, both in order to achieve the highest possible Reynolds' number and to minimize resolution errors in the pressure measurements. Hence, the Reynolds' number based on cavity diameter was and the freestream velocity was monitored at all times using a Pitot-Static tube. All measurements were conducted with the cavity model centre located at 4.29 m downstream of the working section inlet. The relevant boundary layer parameters for the experiments are listed in Table 1.

Table 1. Approach flow parameters used for experiments.

Flow Quantity	Value	Range*
δ	55 mm	± 5 mm
δ_*	7.0 mm	± 0.9 mm
δ_θ	5.1 mm	± 0.7 mm
c_f	0.0030	± 0.0001
u_* / U_0	0.042	± 0.0007

*Range refers to the maximum deviation of a series of measured values measured at a variety of spanwise points across the working section from -1.0D to +1.0D. Quantities stated in the "Values" column are the mean values of these spanwise measurements.

Both the cavity models used for measurements were built of acrylic and had a fixed diameter of 76 mm. The depth of the cavity was adjustable by movement of the piston-like cavity base, although measurements were limited to depths of 0.2, 0.47 and 0.7 D in this study. Figure 3 shows a schematic diagram of the experimental geometry.

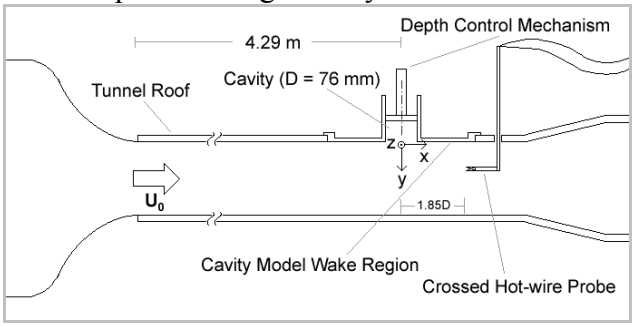

Fig. 3. Schematic diagram of experimental setup (not to scale).

2.2 Surface Pressure Measurements

An acrylic cavity model was fitted with flush-mounted pressure taps to allow the measurement of mean and fluctuating pressures at the cavity surfaces. The pressure taps had an inner diameter of 0.5 mm, and a total of 40 taps were distributed in linear configurations about the cavity surfaces with 10 on the cavity base, a maximum of 12 on the sidewall (depending on the cavity depth), and 16 in the cavity wake region.

These lines of pressure taps were rotated with the cavity model in 10° increments to produce well-resolved mean pressure contours on the cavity surfaces.

The pressures were measured using Honeywell DCAL4 and NDR4 differential pressure transducers with a range of ±1" (25.4 mm) WG and uncertainty of Cp = 0.003, which were sampled at 1,000 Hz / channel for 30 s sample lengths using a PC-controlled data acquisition system. Due to the lengths of tubing used, this pressure measurement apparatus had a frequency response that was constant up to approximately 100 Hz after which it attenuated considerably. Hence, only the low frequency fluctuations were measured accurately with these devices.

From the pressure-time series at each of the measurement points, the mean and RMS values were calculated and charted in the form of contour plots to analyze the patterns in these quantities across the cavity surfaces. The drag due to the presence of the cavity was also calculated by numerically integrating the downstream component of the mean pressures on the cavity sidewall.

2.3 Acoustic Measurements

A separate cavity model of identical geometry and depth variability as the pressure tapped model was built with a series of 13 holes each of 6 mm diameter to flush-mount Panasonic WM-61B miniature electret microphones along the cavity surfaces. The microphones were distributed along the cavity surfaces with 9 on the cavity base, a maximum of 3 on the sidewall (once again, dependent on the cavity depth setting), and 1 on the cavity wake surface. Previous studies by Johnston et. al. [10] and Czech and Savory [11], and have shown that this type of microphone can be successfully used to analyze the frequency spectrum of the fluctuating pressure field when flush-mounted at the cavity surfaces.

These microphones were rotated along with the model at 20° increments in order to record the fluctuating pressure at the model surfaces at a variety of points. Data from the 13 microphones were sampled simultaneously at a rate of 10,000 Hz / channel for 30 second sample lengths, allowing fluctuations from 0 to 5,000 Hz to be resolved. The frequency spectra of the measured pressure data from the microphones was the desired result of these measurements and, since only the fluctuations due to the presence of the cavity were of interest, various filtering techniques were employed to isolate these fluctuations from those due to other sources.

2.4 Wake Velocity Measurements

Velocity measurements were made in the cavity wake by traversing a Dantec 55P61 crossed hot-wire probe through a slot 1.85 D (141 mm) downstream of the cavity model centre, as pictured in Figure 4. Uncertainty for the measured streamwise velocity was always less than 0.4 m/s and uncertainty in the streamwise RMS velocity was always less than 0.09 m/s.

A two-axis traverse moved the probe through a rectangular grid of 66 measurement points (6 rows of 11 spanwise points). The spanwise centre of the grid was lined up with the spanwise centre of the cavity and the points ranged from –D to +D in the spanwise direction (z-axis) and from 0.02D to 0.415D in the vertical direction (y-axis).

The two channels of the hot-wire signal were acquired simultaneously at 20,000 Hz / channel for a sample length of 30 s for each measurement point in the grid. An analog low-pass filter with a corner frequency of 10 kHz was used in all cases to avoid aliasing. Velocity time series were calculated from the hot-wire output and these were used to find the mean and

RMS values for the streamwise velocity, which was the component of greatest interest for this study. To isolate the cavity effect on the wake flow from the background approach flow, the velocity measured with no cavity in place was subtracted from the velocity measured with the cavity model in place.

3 Results and Discussion

3.1 Overview

Mean and fluctuating surface pressures are presented in this section, along with velocity profiles in the cavity wake region and results from the wake flow control experiment. To establish the accuracy of these results, a graph comparing the resulting incremental drag coefficients ($\Delta C_D = C_D - c_f$) measured from the present experiment to similar drag measurements from previous investigations is seen in Figure 5. The present results fit the trend from previous results very well.

3.2 Surface Pressure Measurements

Mean pressure patterns on the cavity surfaces for all three depths tested matched well with previous results published by Hiwada et. al. [7] and Savory et. al. [8]. Contours of Cp_{RMS} were also generated for each of the cavity surfaces from the same data sets as the mean patterns. Figure 6 shows fluctuating pressure contours for h/D = 0.20 and both the sidewall and base images show a remarkable degree of symmetry about the streamwise centreline of the cavity. The intense fluctuation area seen in the sidewall image of Figure 6 centred about $\theta = 180°$ is due to the impingement of the turbulent fluid from the reattachment of the turbulent shear layer on the sidewall at this point. This draws turbulent fluid into the cavity, down the cavity sidewall and drives a reversed flow along the cavity base towards the upstream wall, as evidenced by the high fluctuation levels at the downstream lip with contours perpendicular to the direction of fluid motion.

Figure 7 shows similar images for the h/D = 0.47 case, and a clearly asymmetric flow is demonstrated for this geometry. High fluctuation levels once again mark the shear layer reattachment zone on the downstream cavity sidewall. High fluctuations are also seen on the cavity base at this downstream side, showing that the fluid is being drawn down into the cavity at this location. The flow at this configuration is obviously more complex than for the h/D = 0.20 case and this is demonstrated by the nearly circular-shaped fluctuation maxima on the cavity base near the outer rim at $\theta = 35°$ and on the cavity sidewall slightly more than halfway down, centred at $\theta = 70°$. These circular regions are coincident with circular regions of low pressure in the mean pressure distributions, and these regions are also coincident with swirling regions from surface oil-film pictures taken by Gaudet and Winter [6]. This corroborating evidence suggests that these are points where strong vortex structures are rooted to the cavity surfaces. Evidence from the mean pressure contours and oil-film diagrams also suggests that the vortex rooted to the sidewall at $\theta = 70°$ stretches diagonally across the cavity to the downstream lip of the sidewall at $\theta = 235°$ where the vortex leaves the cavity and convects downstream in the external flow as a trailing vortex. The interaction between this vortex and the one rooted to the cavity base is not yet understood due to a lack of information on the flow inside the cavity away from the surfaces.

Figure 8 shows the fluctuating pressure contours for h/D = 0.70 and, like the h/D = 0.20 case, the distributions are quite symmetric. This geometric configuration shows the lowest pressure fluctuation levels of the three depths tested, suggesting that this case results in the least amount of turbulent external fluid being drawn down into impingement with the cavity surfaces. The more curved nature of the contour lines on the cavity base in the mean pressure distribution (not shown) suggests a more three-dimensional reversed flow along the cavity base (essentially a radial outflow from the downstream edge of the cavity base).

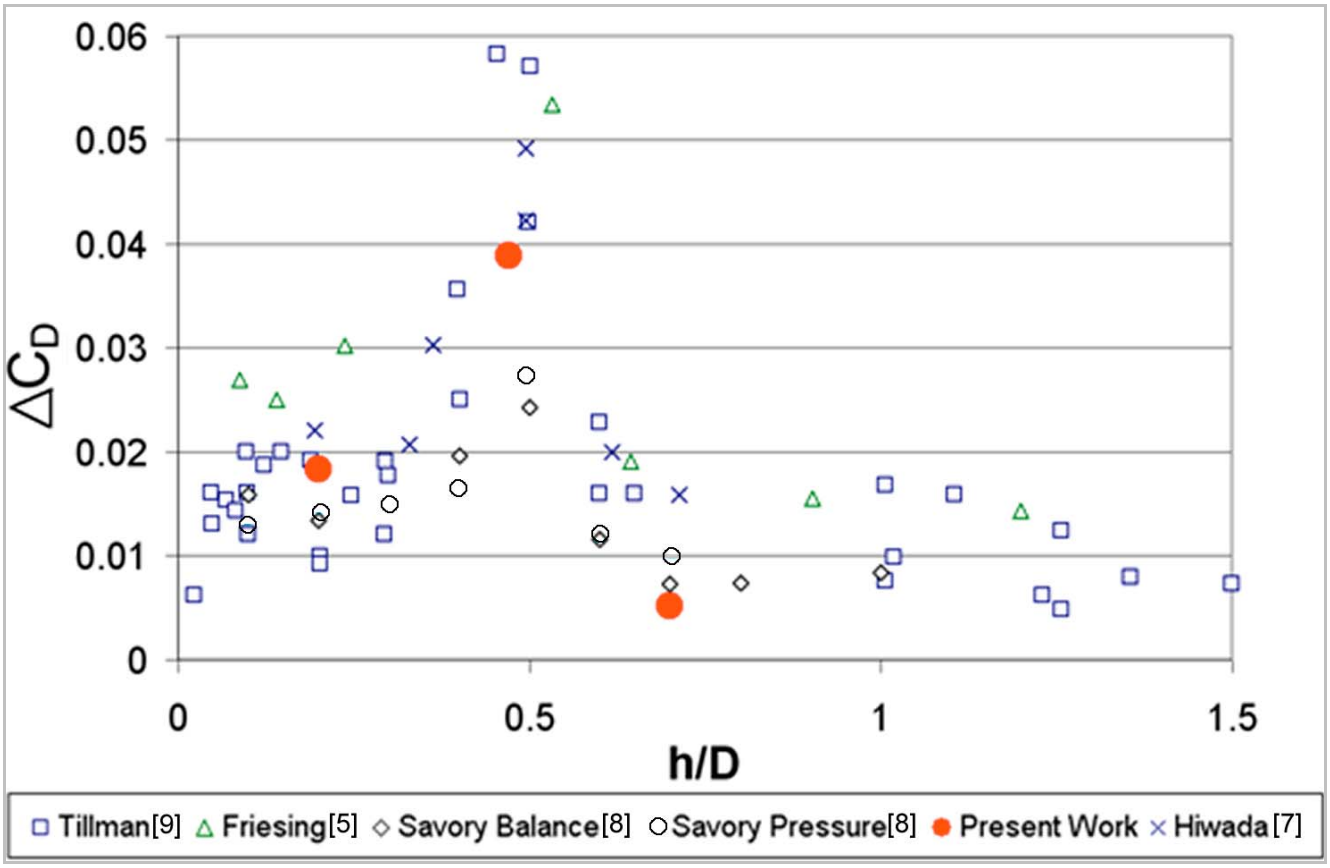

Fig. 4. Comparison of incremental drag coefficient results from present experiment to previous results.

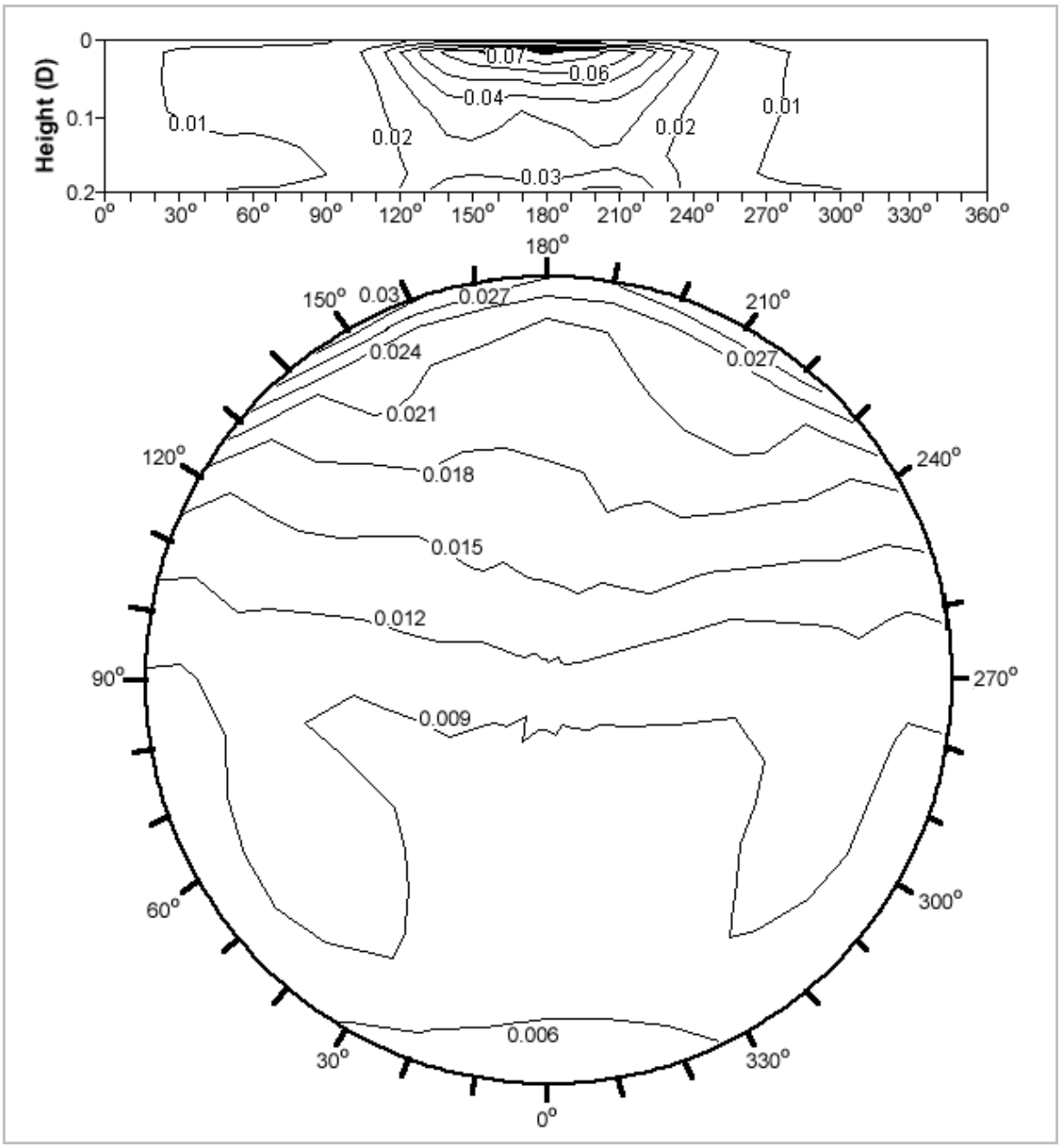

Fig. 5. Fluctuating pressure contours (in units of Cp_{RMS}) on cavity sidewall (top) and base (bottom) for h/D = 0.20.

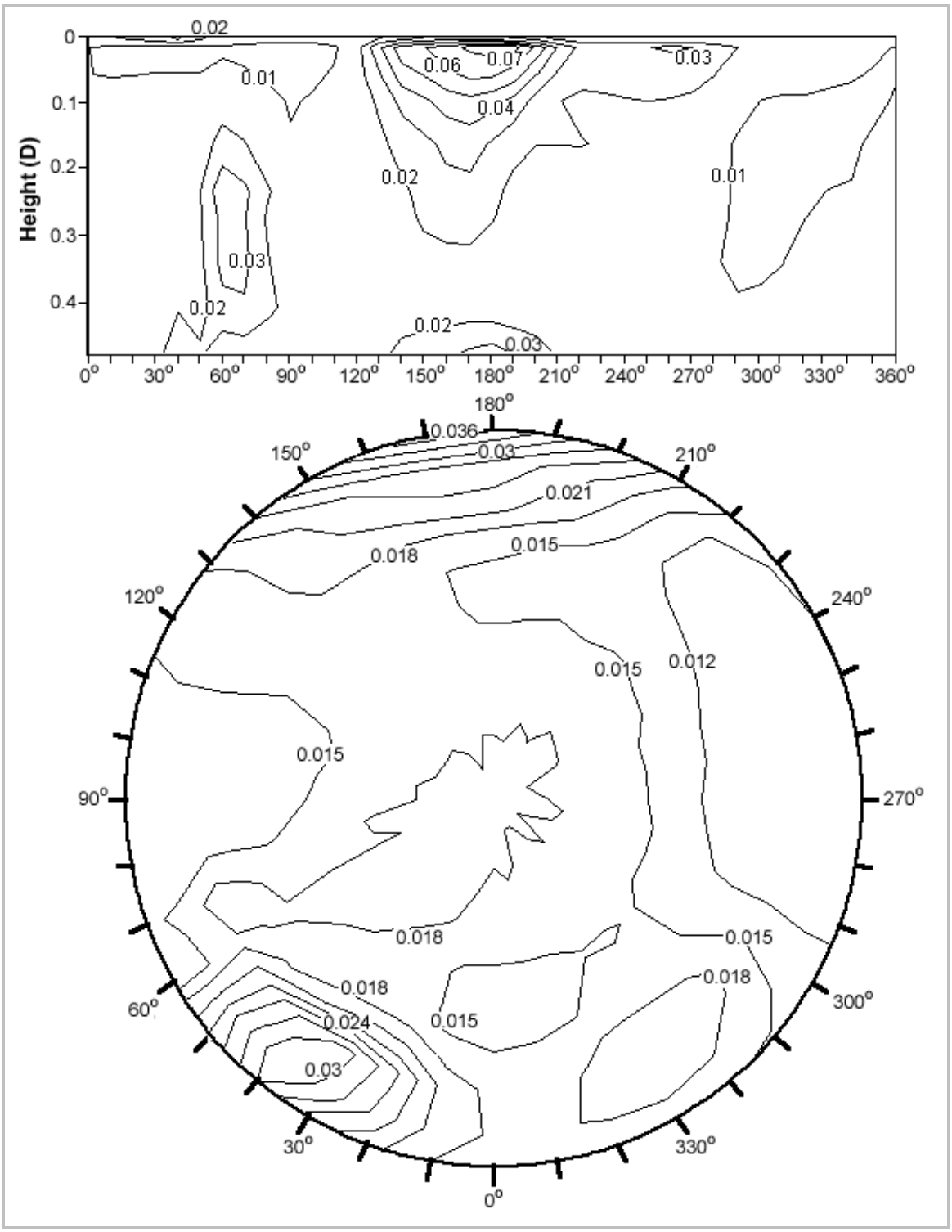

Fig. 6. Fluctuating pressure contours (in units of Cp_{RMS}) on cavity sidewall and base for h/D = 0.47.

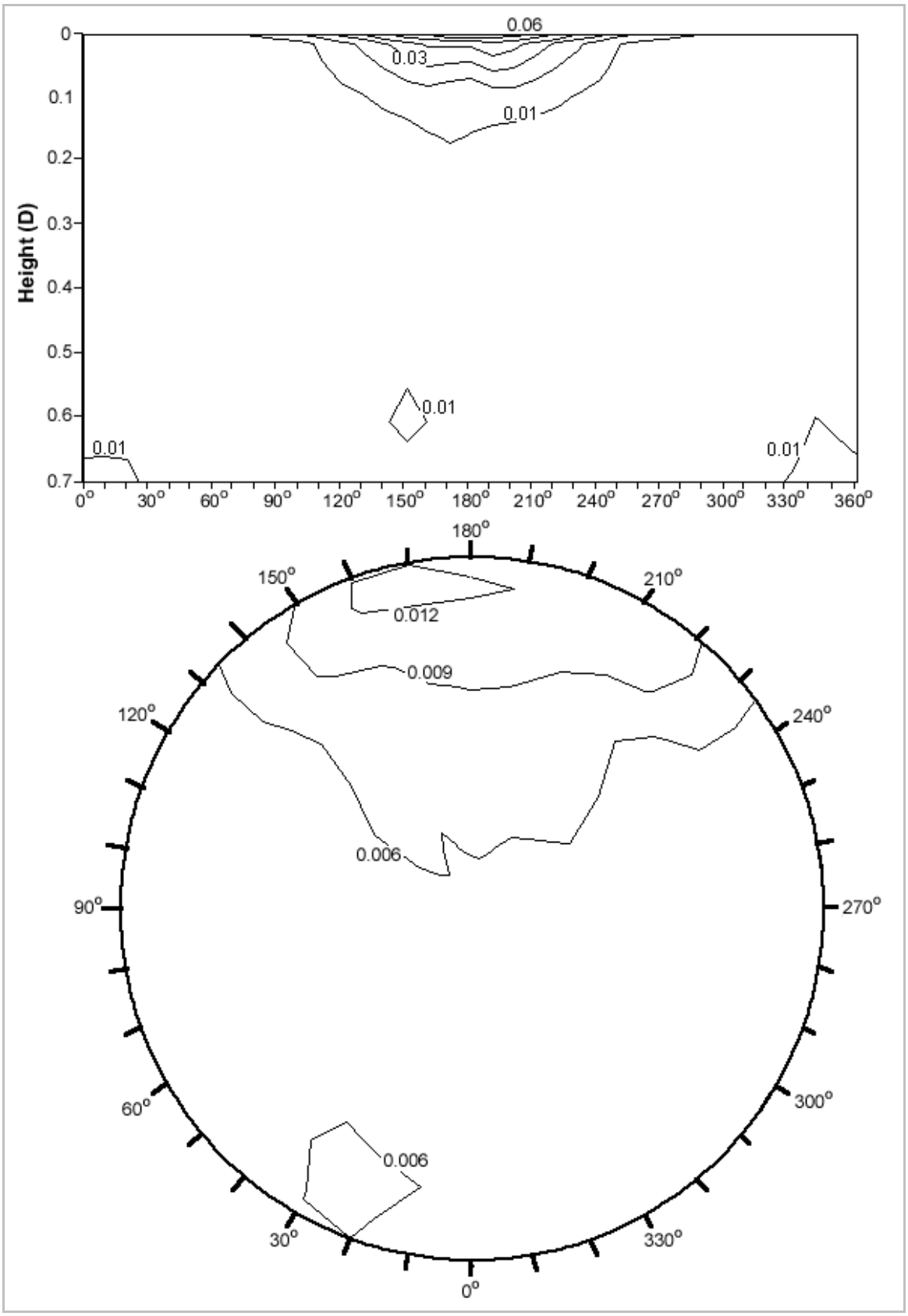

Fig. 7. Fluctuating pressure contours (in units of Cp_{RMS}) on cavity sidewall and base for h/D = 0.70.

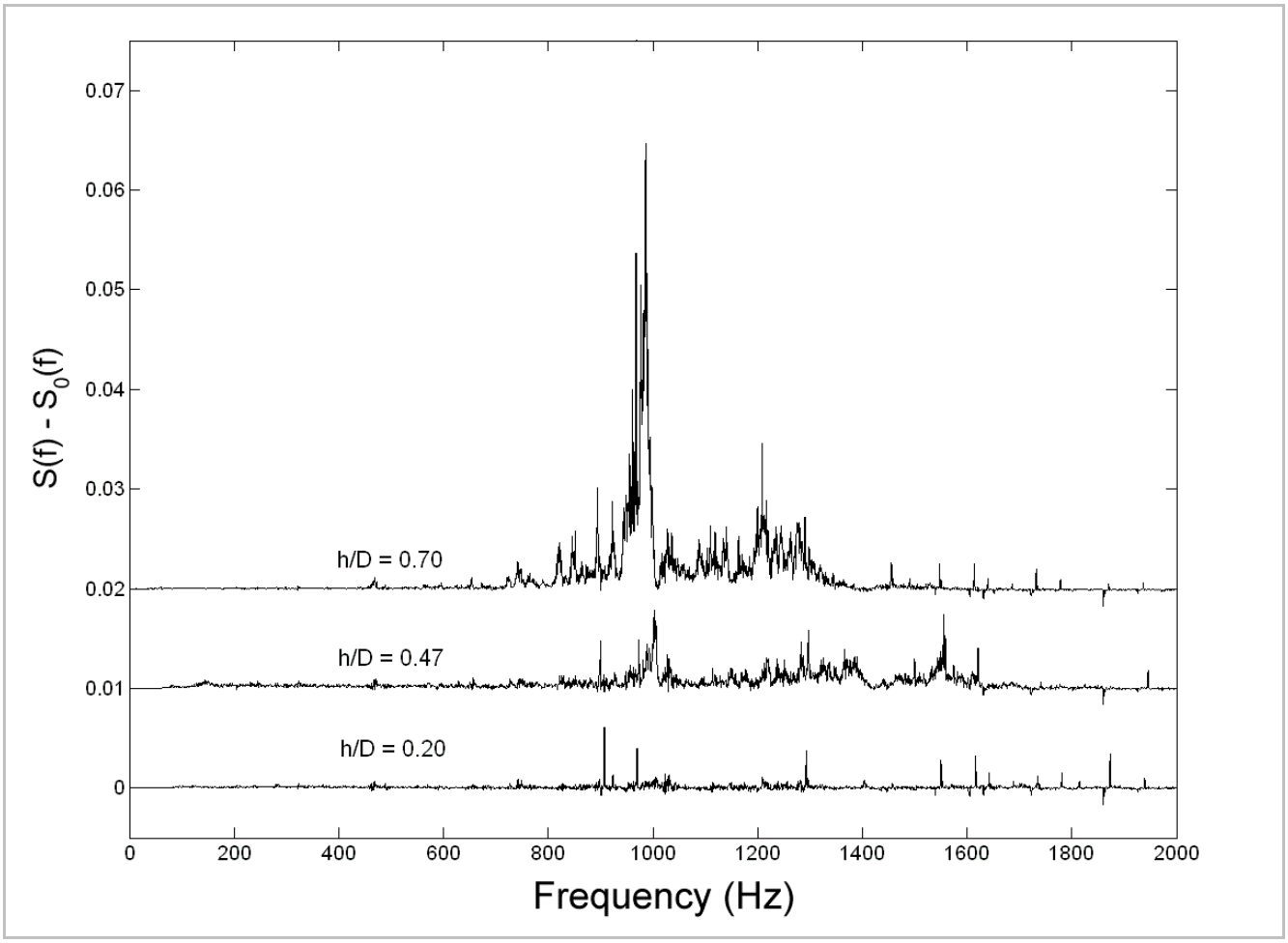

Fig. 8. Wide-band power spectral density plots calculated from data collected by a surface-mounted microphone at centre of cavity model base for three cavity depths: h/D = 0.20, 0.47, 0.70. Plots are offset along the amplitude axis by 0.01, for clarity.

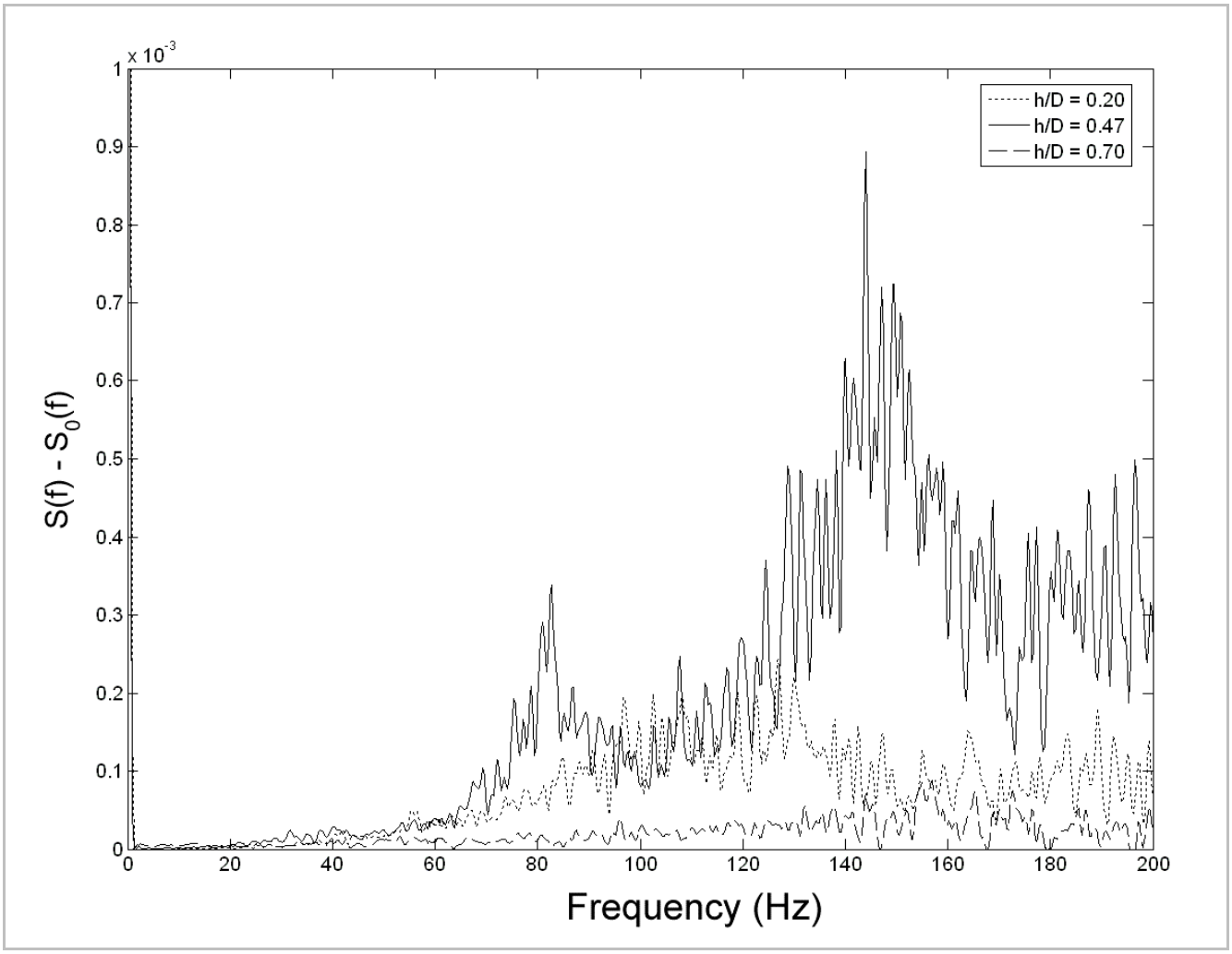

Fig. 9. Superposed narrow-band power spectral density plots calculated from data collected by a surface-mounted microphone at centre of cavity model base for three cavity depths: h/D = 0.20, 0.47, 0.70.

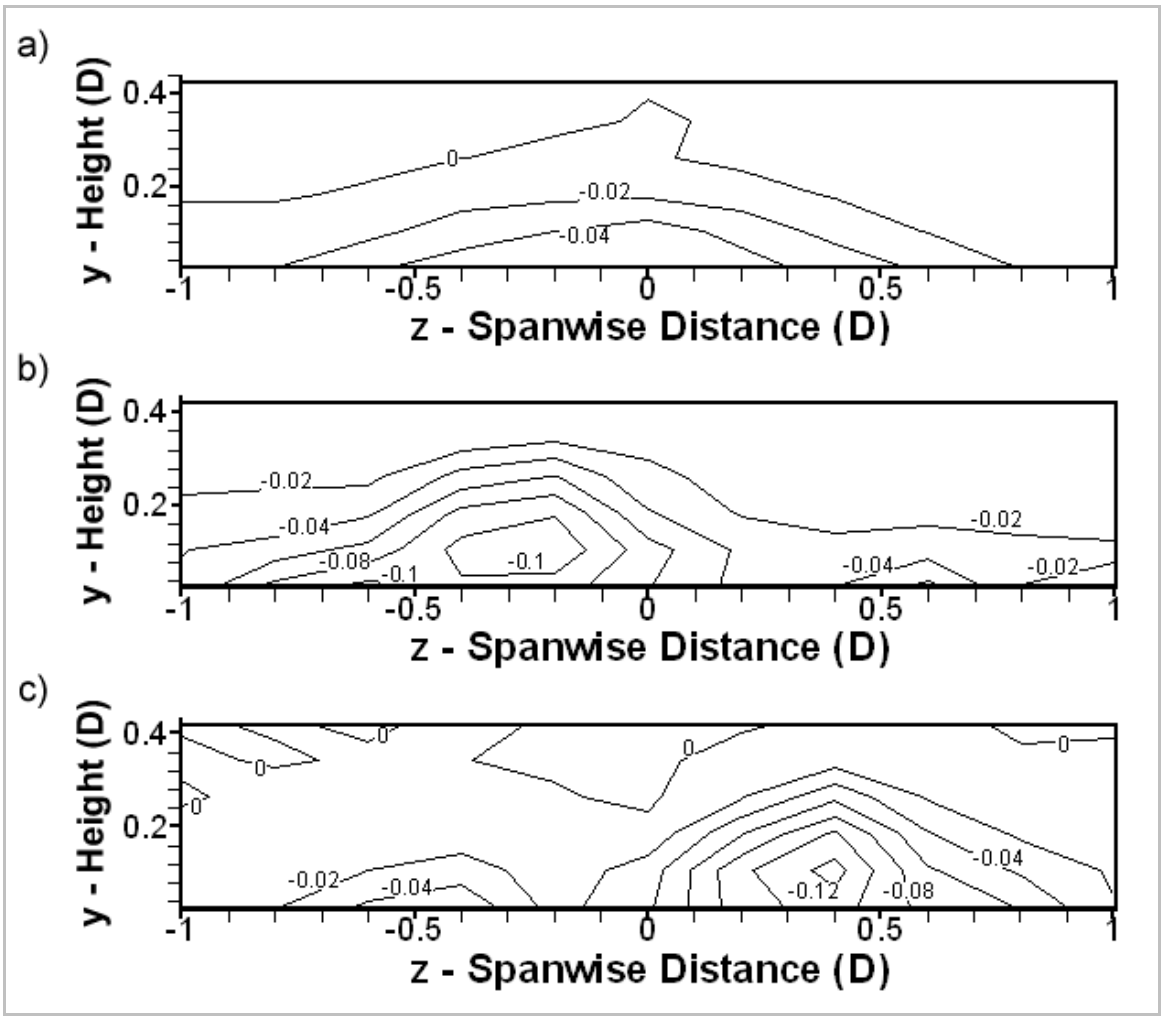

Fig. 10. Contour plots for mean streamwise velocity change, normalized by U_0, in a plane located 1.85D downstream of the cavity model centre. a) cavity depth: h/D = 0.20, b) h/D = 0.47, trailing vortex at left, c) h/D = 0.47, trailing vortex at right.

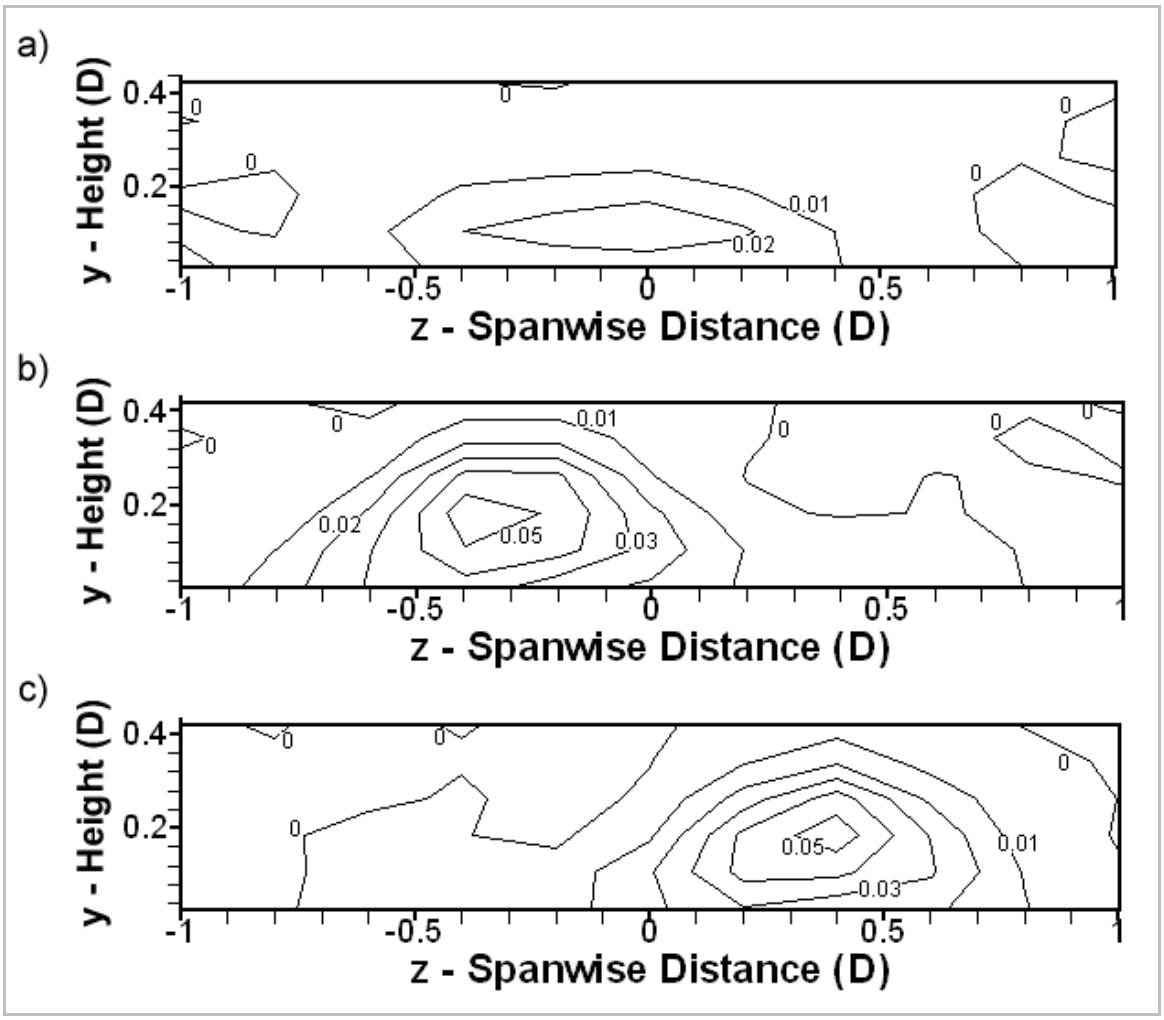

Fig. 11. Contour plots for streamwise RMS turbulence, normalized by U_0, in a plane located 1.85D downstream of the cavity model centre. a) cavity depth: h/D = 0.20, b) h/D = 0.47, trailing vortex at left, c) h/D = 0.47, trailing vortex at right.

3.3 Acoustic Measurements

Peaks in the acoustic spectra measured inside the cavity were expected to be driven by the fluid-dynamic and fluid-resonant mechanisms. Using equation (1) and substituting the cavity diameter D for the variable l, oscillations driven by the fluid-dynamic mechanism would be expected at a frequency of 145.5 Hz for a first mode oscillation, whilst equation (2) predicts frequencies of 2,329 Hz for h/D = 0.20, 1,512 Hz for h/D = 0.47 and 1,164 Hz for h/D = 0.70, for the fluid-resonant mechanism. Power spectral density plots are presented in Figures 8 and 9 for data acquired from a surface-mounted microphone at the centre of the cavity base for the three cavity depths tested. The amplitudes of these plots have been normalized by subtracting the power spectrum obtained by this same microphone with the cavity set to zero depth in order to isolate the cavity flow-related noise from the residual tunnel noise.

The broadband spectra presented in Figure 8 show a high frequency acoustic band in the range of 700 – 1,500 Hz for the deeper cavities tested: h/D = 0.47 and 0.70. These broadband features are likely related to cavity geometry. Although these features have a similar shape for the h/D = 0.47 and 0.70 cases, the h/D = 0.70 case shows increased amplification over a lower frequency band than for h/D = 0.47, due to the greater cavity depth. The features are possibly related to the fluid-resonant oscillation mechanism due to the fact that they give a high amplitude near the predicted frequencies of 1,512 Hz for h/D = 0.47 and 1,164 Hz for h/D = 0.70. This evidence is more pronounced for the h/D = 0.47 case, where a strong peak is centred at 1,545 Hz. The fact that no such feature is seen in the power spectral density (PSD) plot for h/D = 0.20 further indicates that the fluid-resonant mechanism may be the cause of these features, since this type of oscillation is unlikely for shallow cavity depths.

In the lower frequency range (Figure 9), a notable strong peak centred about 147.5 Hz (Strouhal number fD/U_0 = 0.415) is seen in the PSD plot calculated from the data collected by the microphone in the cavity base for h/D = 0.47. This peak is very close to the value of 145.5 Hz (fD/U_0 = 0.410) predicted for the fluid-dynamic oscillation mechanism, which suggests that this peak was indeed caused by cavity feedback resonance. No other depth tested displays this sharp peak, indicating that this feedback resonance may be part of the reason for the asymmetric flow and significantly higher drag observed at this configuration and not at other depths.

3.4 Wake Velocity Measurements

Streamwise velocity and turbulence profiles were acquired in the cavity wake for configurations of h/D = 0.20 and h/D = 0.47. Two profiles were acquired for h/D = 0.47, one for each of the stable states for this cavity flow. Once again, an attempt was made to isolate the cavity effect on the flow from the approach flow of the cavity. To do this, similar profiles were measured at the same measurement points with no cavity in place (h/D = 0.00) and the mean and turbulent statistics calculated from these data were subtracted from the cases with the cavity in place. The resulting values were normalized by the free stream velocity U_0 to display the cavity effects in terms of the velocity of the approach flow to form the mean velocity unit $\Delta\overline{u}$ and the turbulent quantity Δu_{RMS}. These figures are presented in Figures 10 and 11.

Figures 10 b and c are both wake velocity profiles taken behind the cavity for h/D = 0.47. The resulting profiles are nearly mirror images of one another due to the existence of two marginally stable states for the cavity flow at this configuration. The flow could be switched between these two states by momentarily introducing a flat rectangular board into the working section upstream of the cavity such that it was normal to the free stream. It was also found that the exposed board area, spanwise board location and duration of blockage were all factors in determining

whether or not the flow would switch. It is clear that the h/D = 0.47 case caused the greatest mean streamwise velocity deficit, reaching a maximum of 11.6% of U_0 for the profile centred at z = 0.35D (Figure 11c). The profiles assumed the expected qualitative appearance, with those for h/D = 0.20 (Figures 10a and 11a) being quite symmetric about the spanwise centre and the h/D = 0.47 cases (Figures 10b,c and 11b,c) being very asymmetric. Also, the nearly circular features in the plots for h/D = 0.47, centred at z = +/- 0.35 D depending on the sense of the flow, are evidence of the presence of the trailing vortex convected from the downstream edge of the cavity for this configuration. These features are then cross sections of the trailing vortex in this plane. In all cases, regions of high mean streamwise velocity loss are coincident with regions of high streamwise turbulence intensity, showing the conversion of energy from the mean streamwise velocity into turbulent kinetic energy. As expected, for the h/D = 0.20 case, the regions of high mean streamwise velocity loss and turbulence intensity are found almost exclusively in the spanwise range of the cavity, from z = -0.5D to +0.5D, showing that these wake features are a result of the cavity presence.

4 Conclusions

The nature of the fluctuating flow field associated with cavities of circular planform has been clarified. Regions of intense surface pressure fluctuation coincide with shear layer reattachment zones and wall-rooted vortex centres observed from mean pressure profiles. Low frequency oscillations are measured inside the cavity for the more shallow cavity depths tested (h/D = 0.20, 0.47), due to the strong entrainment of external turbulent fluid into the cavity at these configurations. A particularly strong peak noted at 147.5 Hz for the h/D = 0.47 configuration is quite likely due to the fluid-dynamic cavity feedback resonance mechanism, and, not being observed at other depths, this oscillation could be a cause of the asymmetric flow and high drag noted for this configuration. In order to improve the support for this explanation, a frequency analysis of the oscillating pressures on the cavity surfaces should be carried out for a greater range of cavity depths from h/D = 0.1 to 1.0 to see if only configurations for which h/D 0.5 exhibit this strong peak at the frequency predicted for cavity feedback resonance. Broadband high frequency oscillations are noted for the deeper cavities (h/D = 0.47 and 0.70) suggesting the presence of an oscillation mechanism that is dependent on cavity depth.

For aerodynamic applications it seems best to keep circular cavities to dimensions of h/D 0.3, as cavities fitting this requirement have been noted by previous investigators to have a low drag coefficient and such cavities have been observed in the present study to produce a great deal less high-frequency acoustic noise than deeper cavities.

Further evidence has been found for the existence of a trailing vortex structure for h/D = 0.47 with the appearance of a circular cross-section region of the vortex in the turbulence intensity measured downstream of the cavity model offset from the cavity centre, and a similarly located mean streamwise velocity deficit region has also been measured.

Nomenclature

c	Local speed of sound
c_f	Local skin friction coefficient
Cp	Pressure coefficient
Cp_{RMS}	Fluctuating pressure coefficient
D	Cavity diameter
f	Frequency of oscillation

h	Cavity depth
l	Streamwise length of a rectangular cavity
m	Integer mode number
M	Free stream Mach number
N	Odd integer mode number
p	Measured pressure
p_s	Static pressure
S(f)	Power Spectral Density
u_*	Friction velocity
U_0	Free stream velocity
x	Streamwise co-ordinate, origin at cavity centre
y	Vertical co-ordinate, origin at cavity lip
z	Spanwise co-ordinate, origin at cavity centre
δ	Boundary layer thickness
δ_*	Displacement thickness
δ_θ	Momentum thickness
ΔC_D	Incremental drag coefficient
$\Delta\overline{u}$	Cavity effect on mean streamwise velocity, normalized by U_0
Δu_{RMS}	Cavity effect on streamwise RMS velocity, normalized by U_0
γ	Vortex impingment / acoustic tone lag factor
κ	Ratio of vortex convection velocity to free stream velocity
θ	Angular co-ordinate, 0^o at upstream side of cavity, 180^o at downstream side
ρ	Density of air
τ_w	Wall shear stress

References

[1] Rossiter, J. E., Wind-Tunnel Experiment on the Flow over Rectangular Cavities at Subsonic and Transonic Speeds. *British ARC R&M* No. 3428, 1964.

[2] Ukeiley, L., Murray, N., Velocity and Surface Pressure Measurements in an Open Cavity. *Experiments in Fluids*, Vol. 38, pp. 656-671, 2005.

[3] McGregor, O. W., White, R. A., Drag of Rectangular Cavities in Supersonic and Transonic Flow Including the Effects of Cavity Resonance,. *AIAA Journal*, Vol. 8, pp. 1959-1964, 1970.

[4] Sen, S.N., *Acoustics - Waves and Oscillations*. Wiley Eastern Ltd., 1990.

[5] Friesing, H., Measurement of the drag associated with recessed surfaces: cut-outs of rectangular and elliptical planform. *Z.W.B.F.B.*, No. 628 (RAE Library Translation 1614, 1971), 1936.

[6] Gaudet, L., Winter, K.G., Measurements of the drag of some characteristic aircraft excrescences immersed in turbulent boundary layers. *RAE Tech Memo Aero*, No. 1538 (also *AGARD*, No. CP124, 1973), 1973.

[7] Hiwada, M., Kawamura, T., Mabuchi, I., Kumada, M., Some Characteristics of the Flow Pattern and Heat Transfer past a Circular Cylindrical Cavity. *Bulletin of the JSME*, Vol. 26, No. 220, pp. 1744-1752, 1983.

[8] Savory, E., Toy, N., Gaudet, L., Effect of lip configuration on the drag of a circular cavity. *Emerging Techniques in Drag Reduction*,

Mechanical Engineering Publications Ltd., 317-335, 1996.

[9] Tillman, W., Additional measurements of the drag of surface irregularities in turbulent boundary layers. *NACA*, No. TM 1299 (also in "New resistance measurements with surface irregularities in the turbulent boundary layer:, *Forschungshefte fur Schiffstechnik*, Vol. 2, pp. 81-88, (BSRA Trans No. 322), 1953), 1951.

[10] Johnston, R. T., Sullivan, J. P., An inexpensive pressure transducer for the measurement of low amplitude unsteady pressure signals. *Experiments in Fluids*, Vol. 16, pp. 342-344, 1994

[11] Czech, M., Savory, E., Toy, N., Mavrides, T., Flow regimes associates with yawed rectangular cavities. *Aeronautical Journal*, Vol. 105, No. 1045, pp. 125-134, 2001.